We are IntechOpen,
the world's leading publisher of
Open Access books
Built by scientists, for scientists

6,900
Open access books available

185,000
International authors and editors

200M
Downloads

154
Countries delivered to

Our authors are among the

TOP 1%
most cited scientists

12.2%
Contributors from top 500 universities

CLARIVATE ANALYTICS
BOOK CITATION INDEX
INDEXED

WEB OF SCIENCE™

Selection of our books indexed in the Book Citation Index
in Web of Science™ Core Collection (BKCI)

Interested in publishing with us?
Contact book.department@intechopen.com

Analysis of Wireless Power System Efficiency in Dependency on Configuration of Resonant Tank

Michal Frivaldsky, Pavol Spanik, Peter Drgona,
Viliam Jaros and Marek Piri

Abstract

This chapter compares various compensation methods for resonant coupling of the wireless energy transfer system. A proposed analysis is particularly relevant to any application where contactless battery charging is used. Main parameters that are investigated include efficiency and electrical variables (current and voltage) of the circuit. In order to analyze the most suitable solution of coupling compensation, the relevant equations are graphically interpreted for each discussed circuit topology. Finally, this chapter provides the recommendations how to design the wireless power-transfer system with the highest possible efficiency for the given system parameters (switching frequency and transmitting distance).

Keywords: Efficiency, wireless power transfer, configuration, resonant compensation, distance

1. Introduction

Nowadays, electrically powered automobiles show higher interest in the automotive industry. Electric vehicles gain this interest thanks to high efficiency. In the case of the asynchronous motor, the electrical energy can be converted into the mechanical with an efficiency of 90%, which is much more than the efficiency of the combustion engine that has an efficiency of only 25–34%. Due to the limitation of natural resources such as petroleum and natural gas, the power electronics and energy conversion along with the development of new battery types contribute to the development and application in the automotive industry. The main disadvantage of the electric car is the energy accumulation. Batteries are large, heavy, with short lifetime, and

long charging times. These reasons show how necessary it is to solve an issue of battery charging [1]. In general, charging systems can be classified as wired and these could be replaced with wireless (inductive) systems.

Wireless power transfer and issues relevant to wireless charging of various types of electronic devices are still important and emerging trends in electrical engineering [2–4]. Regarding of wireless power transfer, each application requires several self-specific operational properties or transfer characteristics. The most important of them are transmitting efficiency, value of the output power, mutual position between the transmitter and the receiver, and their geometric dimensions. One possible way how to influence these parameters lies in the main circuit configuration of a compensation network of the wireless energy transfer (WET) system. Inductively coupled power-transfer systems have been suited for a wide spectrum of consumer applications including electromobility (battery charging of vehicles). Even high system efficiency has been achieved (approximately 70%); however, the restriction to close range, typically shorter than 30% of the coil diameter, is the main limitation for perspective usage in high-efficiency or high-performance systems [5, 6].

It the beginning of 2000s, a team of researchers under charge of Prof. Soljacic introduced a new concept of strongly coupled magnetic resonance for wireless energy transfer systems [7]. In comparison with an inductively coupled system, the coils with resonant inductive coupling have several significant advantages. The most important of them are as follows: the coupling may be very efficient even at large transmission distances, it has low environmental impact, and can be variously tuned/configured based on the requirements of target application. The solution of the WET system based on the magnetic-resonance coupling represents constantly investigated phenomena. Most of the analyses are based on the pure theory of physical interactions, which are unable to provide clear and consistent overview of knowledge for researchers in the field of electrical engineering [8, 9]. Based on this, it can be said that some important relationships between system efficiency, amount of transmitted power, and transmitting distance for magnetic-resonance coupled WET systems need to be introduced.

This chapter describes a simple equivalent circuit model for magnetic-coupled and resonant magnetic-coupled WET systems. The resonant coupling is further described in details, whereby all key system equations for various configurations of a resonant compensation network with pure resistive load are derived. From the component design point of view, it is also important to have knowledge about values of voltage and current in the main circuit. In the last part of the chapter, the general recommendations for practical use of each variant are provided.

2. Nonresonant magnetic coupling of the WET system

In the case of nonresonant magnetic coupling, the system acts as an air-cored transformer with relatively low mutual inductance. Due to high supplying frequency, the primary and the secondary leakage reactance cause a significant voltage drop, which limits amount of power

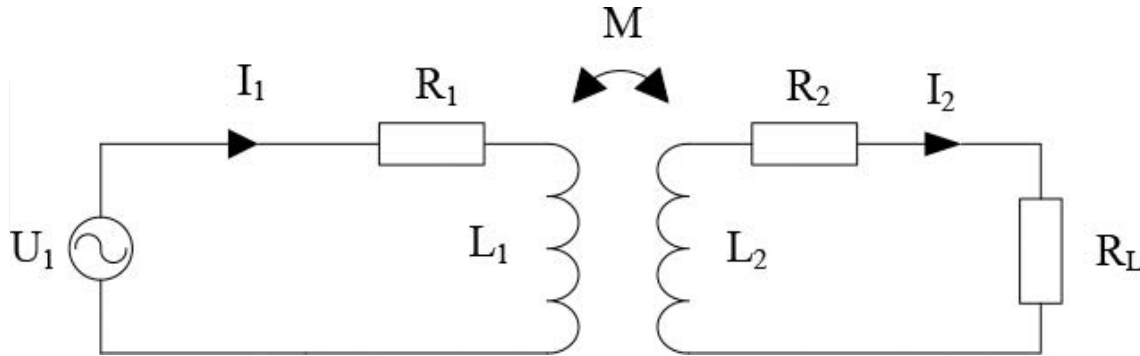delivered to the load. Equivalent circuit composed for this type of coupling is shown in **Figure 1**.

Figure 1. Equivalent circuit of the inductively coupled nonresonant WET system.

The circuit can be completely described by the system of loop currents calculated by Eq. (1):

$$\begin{bmatrix} \dot{U}_1 \\ 0 \end{bmatrix} = \begin{bmatrix} R_1 + j\omega L_1 & -j\omega M \\ -j\omega M & R_2 + R_L + j\omega L_2 \end{bmatrix} \cdot \begin{bmatrix} \dot{I}_1 \\ \dot{I}_2 \end{bmatrix} \tag{1}$$

The parameters R_1 and R_2 represent parasitic resistances of transmitting and receiving coils with self-inductances L_1 and L_2, M forms the mutual inductance between respective coils, and R_L is the load (purely resistive). With regard to the high operational frequencies, the switched power source with square-wave voltage should be used to supply the system. In this case, Eq. (1) needs to be rewritten in Eq. (1) to consider selected frequency spectrum.

$$\begin{bmatrix} \dfrac{4}{\pi} \displaystyle\sum_{k=1,3,5,..}^{\infty} \dfrac{\dot{U}_1}{k} \\ 0 \end{bmatrix} = \begin{bmatrix} \displaystyle\sum_{k=1,3,5,..}^{\infty} R_1 + jk\omega L_1 & \displaystyle\sum_{k=1,3,5,..}^{\infty} -jk\omega M \\ \displaystyle\sum_{k=1,3,5,..}^{\infty} -jk\omega M & \displaystyle\sum_{k=1,3,5,..}^{\infty} R_2 + R_L + jk\omega L_2 \end{bmatrix} \cdot \begin{bmatrix} \dot{I}_1 \\ \dot{I}_2 \end{bmatrix} \tag{2}$$

On the other hand, the uncompensated leakage reactance forms in the circuit with a very high impedance even for a lower frequency component. This impedance causes a significant voltage drop and therefore the contribution of this harmonic component is very low. The system can be therefore analyzed only for the fundamental wave while keeping relatively good accuracy. The winding currents derived for the fundamental wave are provided in Eqs. (3) and (4):

$$\dot{I}_1 = \frac{R_2 + R_L + j\omega L_2}{(R_1 + j\omega L_1).(R_2 + R_L + j\omega L_2) + (\omega M)^2} \dot{U}_1 \tag{3}$$

$$\dot{I}_2 = \frac{-j\omega M}{(R_1 + j\omega L_1).(R_2 + R_L + j\omega L_2) + (\omega M)^2}\dot{U}_1 \tag{4}$$

The input power can be counted from the complex power on the primary side (5):

$$P_{IN} = \Re\{\dot{U}_1.\dot{I}_1^*\} \tag{5}$$

The secondary side average power is then found using the loading resistance and the current flowing through it (Eq. (6)):

$$P_{OUT} = R_L.\left|\dot{I}_2\right|^2 = R_L.\left|\frac{-j\omega M}{(R_1 + j\omega L_1).(R_2 + R_L + j\omega L_2) + (\omega M)^2}\dot{U}_1\right|^2 \tag{6}$$

The transmitting efficiency (7) is further given by the ratio of the output power (6) and the input power (5):

$$\eta = \frac{P_{OUT}}{\left|\dot{S}_{IN}\right|.\cos(\varphi)} = \left|\frac{R_Z\omega^2 M^2}{\left[(R_1 + j\omega L_1).(R_2 + R_L + j\omega L_2) + (\omega M)^2\right].(R_2 + R_L + j\omega L_2).\cos(\varphi)}\right| \tag{7}$$

where

$$\cos(\varphi) = \frac{\Re(\dot{S}_{IN})}{\left|\dot{S}_{IN}\right|} = \frac{\Re\left(\dfrac{R_2 + R_L + j\omega L_2}{(R_1 + j\omega L_1).(R_2 + R_L + j\omega L_2) + (\omega M)^2}\dot{U}_1^2\right)}{\left|\dfrac{R_2 + R_L + j\omega L_2}{(R_1 + j\omega L_1).(R_2 + R_L + j\omega L_2) + (\omega M)^2}\dot{U}_1^2\right|} \tag{8}$$

The simulation parameters are taken from two constructed experimental prototypes of coupling coils, which are also identical. Their values are therefore the same on the primary as well as on the secondary side. The self-inductance equals $L_1 = L_2 = 127.4$ µH, parasitic resistance $R_1 = R_2 = 0.447$ Ω, and the load $R_L = 8$ Ω. The analyzed frequency range ($f_{range} = 290–340$ kHz) is set according to the resonant frequency obtained from the resonant magnetic coupling discussed in the following chapter. The used compensation capacitors also have the same capacities $C_1 = C_2 = 2$ nF. In the simulation, the minimal mutual inductance $M_{min} = 1$ µH corresponds to the transmitting distance of 50 cm, whereas its maximal value $M_{max} = 11$ µH represents the distance of 25 cm. This transmitting range is selected based on the application area, i.e., +battery charging of electric vehicles.

The results from simulation of the inductively coupled WET system plotted against frequency and mutual inductance are shown in **Figures 2–4**. The waveforms of the input and output powers are shown in **Figure 2**, the source and load current are shown in **Figure 3**, and the efficiency calculated using Eq. (7) together with a secondary induced voltage U_{L2} are shown in **Figure 4**.
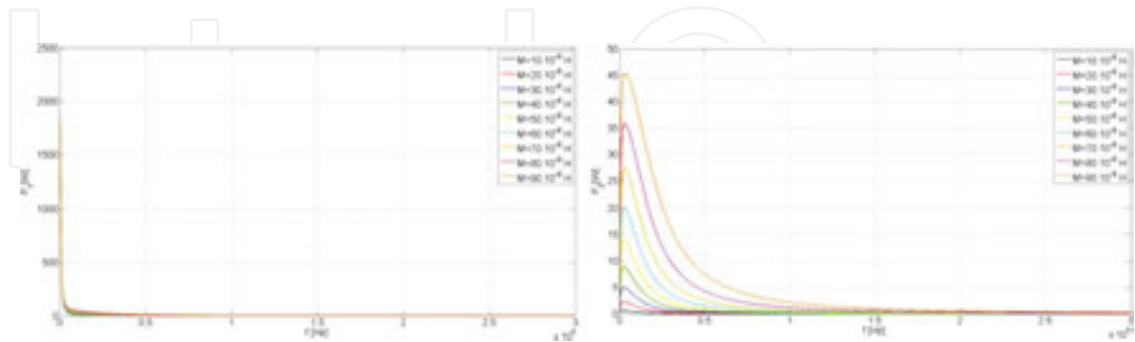

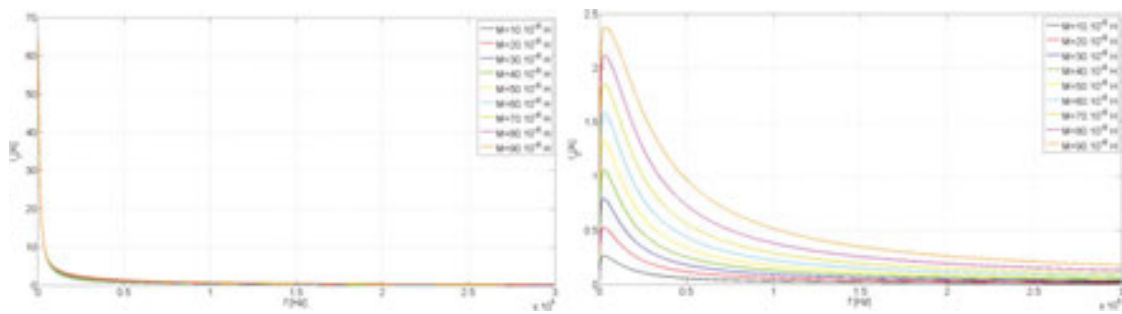**Figure 2.** Input power (left) and output power (right) dependency on nonresonant coupling.

Figure 3. Source current (left) and load current (right) dependency on nonresonant coupling.
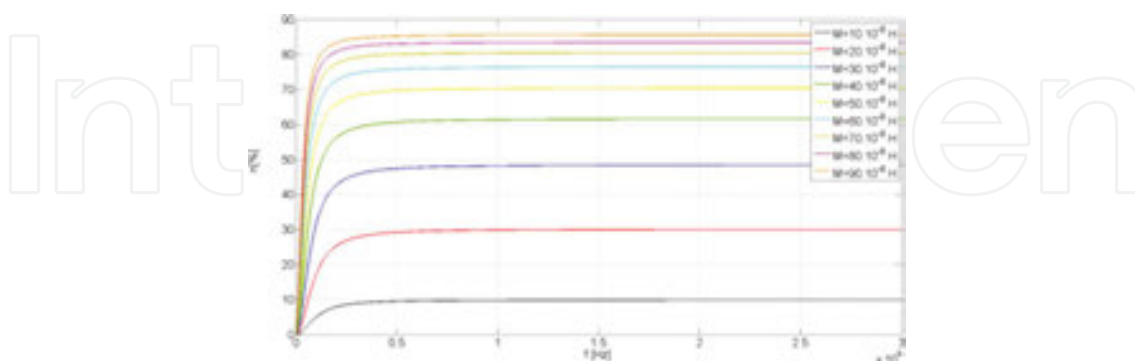

Figure 4. Efficiency dependency on nonresonant coupling.

As it can be seen from **Figure 4** (right), the transmitting efficiency mainly varies with given mutual inductance. The system is practically independent of frequency change even for the whole considered frequency range.

3. Series–series resonant coupling of the WET system

For series–series compensation, the capacitor is connected in series with transmitting and receiving coils (**Figure 5**).
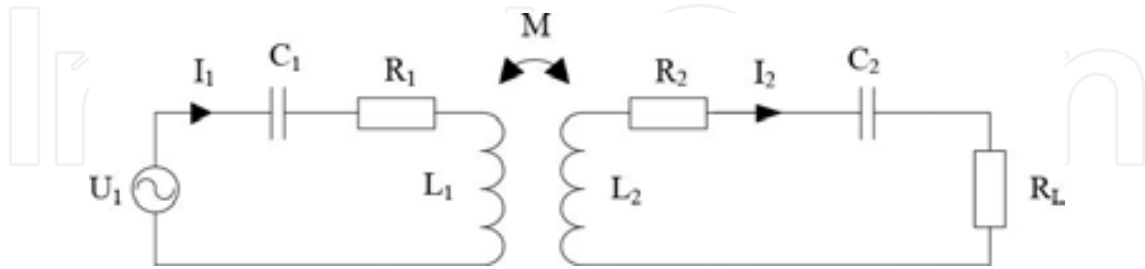

Figure 5. Equivalent circuit of the series–series compensated WET system.

Mathematical model of series–series compensation is, from the point of view of complexity, much easier than other compensation types. Using the methodology of loop currents, the impedance matrix of this configuration can be expressed as follows (11):

$$\left[R_1 + j\left(\omega L_1 - \frac{1}{\omega C_1} \right) \right].\dot{I}_{1\_SS} - j\omega M.\dot{I}_{2\_SS} = \dot{U}_{1\_SS} \tag{9}$$

$$-j\omega M.\dot{I}_{1\_SS} + \left[R_2 + R_L + j\left(\omega L_2 - \frac{1}{\omega C_2} \right) \right].\dot{I}_{2\_SS} = 0 \tag{10}$$

$$\begin{bmatrix} \dot{U}_{1\_SS} \\ 0 \end{bmatrix} = \begin{bmatrix} R_1 + j\left(\omega L_1 - \frac{1}{\omega C_1} \right) & -j\omega M \\ -j\omega M & R_2 + R_L + j\left(\omega L_2 - \frac{1}{\omega C_2} \right) \end{bmatrix} \cdot \begin{bmatrix} \dot{I}_{1\_SS} \\ \dot{I}_{2\_SS} \end{bmatrix} \tag{11}$$

From (11), the formula for the current of the transmitting and receiving parts in the complex form as (12) and (13) can be derived:

$$\dot{I}_1 = \dot{I}_{1\_SS} = \frac{R_2 + R_L + j\left(\omega L_2 - \frac{1}{\omega C_2} \right)}{\left[R_1 + j\left(\omega L_1 - \frac{1}{\omega C_1} \right) \right] \cdot \left[R_2 + R_L + j\left(\omega L_2 - \frac{1}{\omega C_2} \right) \right] + (\omega M)^2} \dot{U}_{1\_SS} \tag{12}$$

$$\dot{I}_2 = \dot{I}_{2\_SS} = \frac{-j\omega M}{\left[R_1 + j\left(\omega L_1 - \dfrac{1}{\omega C_1}\right)\right]\cdot\left[R_2 + R_L + j\left(\omega L_2 - \dfrac{1}{\omega C_2}\right)\right] + (\omega M)^2}\dot{U}_{1\_SS} \tag{13}$$

If the circuit is supplied by harmonic voltage with a frequency equal to the resonant frequency, then the value of the capacitive and inductive parts of the complex impedance will be the same and can be subtracted. Then, for the previous formulas (14) and (15), the following conditions are valid:

$$\dot{I}_1 = \dot{I}_{1\_SS} = \frac{R_2 + R_L}{R_1 R_2 + R_1 R_L + (\omega M)^2}\dot{U}_{1\_SS} \tag{14}$$

$$\dot{I}_2 = \dot{I}_{2\_SS} = \frac{-j\omega M}{R_1 R_2 + R_1 R_L + (\omega M)^2}\dot{U}_{1\_SS} \tag{15}$$

Equations (14) and (15) show that the circuit during resonance has only resistive characteristics, and circuit currents are given just by the parasitic resistances of coils, load resistance, and supply voltage. The input and output powers of the circuit with –series–series compensation can be expressed as Eqs. (16) and (17). The graphical interpretation of Eq. (17), as plotted in **Figure 6**, shows that the operation of the system with this kind of compensation should be excluded from resonant point. In other case, for low values of M (high distance of coils), the input power, as well as the output power (output current), rises too sharply, which might destroy the whole system.

$$\dot{S}_{IN\_SS} = \dot{I}_1 \dot{U}_{1\_SS} = \frac{R_2 + R_L + j\omega L_2}{\left[R_1 + j\left(\omega L_1 - \dfrac{1}{\omega C_1}\right)\right]\cdot\left[R_2 + R_L + j\left(\omega L_2 - \dfrac{1}{\omega C_2}\right)\right] + (\omega M)^2}\dot{U}_{1\_SS}^2 \tag{16}$$

$$P_{OUT\_SS} = R_L\cdot|I_2|^2 = R_L\cdot\left|\frac{-j\omega M}{\left\{\left[R_1 + j\left(\omega L_1 - \dfrac{1}{\omega C_1}\right)\right]\cdot\left[R_2 + R_L + j\left(\omega L_2 - \dfrac{1}{\omega C_2}\right)\right] + (\omega M)^2\right\}}\dot{U}_{1\_SS}\right|^2 \tag{17}$$

Dependence of efficiency for the series–series compensated circuit in the frequency domain can be expressed using Eq. (18):

$$\eta = \frac{\dot{P}_{OUT\_SS}}{\dot{S}_{IN\_SS}.\cos(\varphi)}$$

$$= \frac{R_L \omega^2 M^2}{\left\{\left[R_1 + j\left(\omega L_1 - \frac{1}{\omega C_1}\right)\right].\left[R_2 + R_L + j\left(\omega L_2 - \frac{1}{\omega C_2}\right)\right] + (\omega M)^2\right\}.(R_2 + R_L + j\omega L_2).\cos(\varphi)} \tag{18}$$

where

$$\cos(\varphi) = \frac{\Re\left(\dot{S}_{IN}\right)}{\left|\dot{S}_{IN}\right|} = \frac{\Re\left(\dfrac{R_2 + R_L + j\omega L_2}{\left[R_1 + j\left(\omega L_1 - \dfrac{1}{\omega C_1}\right)\right].\left[R_2 + R_L + j\left(\omega L_2 - \dfrac{1}{\omega C_2}\right)\right] + (\omega M)^2}\dot{U}_{1\_SS}^2\right)}{\left|\dfrac{R_2 + R_L + j\omega L_2}{\left[R_1 + j\left(\omega L_1 - \dfrac{1}{\omega C_1}\right)\right].\left[R_2 + R_L + j\left(\omega L_2 - \dfrac{1}{\omega C_2}\right)\right] + (\omega M)^2}\dot{U}_{1\_SS}^2\right|} \tag{19}$$
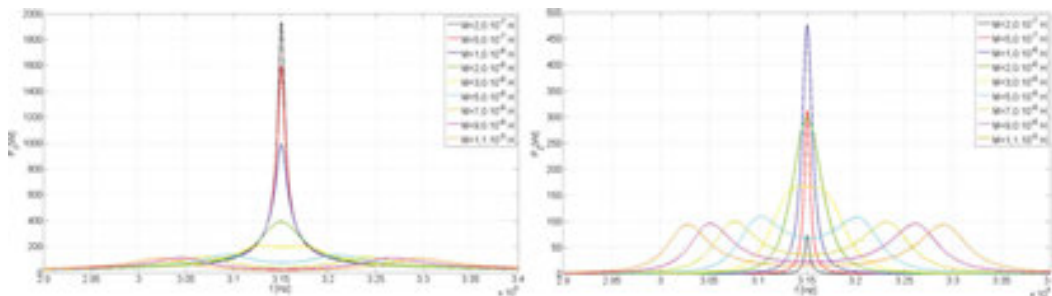

Figure 6. Input power (left) and output power (right) dependency on series–series coupling.

The highest efficiency can be achieved at the resonant frequency. Its value is above 90% when higher values of mutual inductance are considered. The main disadvantage of high efficiency achievement is that for a given value of *M*, the transmitted power is too low (**Figure 6**, right). This fact is crucial when simultaneously high efficiency together with high power transfer is required. The solution is to operate the system at the frequency which is given by Eq. (20).

$$\left[R_1 + j\left(\omega L_1 - \frac{1}{\omega C_1}\right)\right].\dot{I}_{1\_SP} - j\omega M.\dot{I}_{2\_SP} = \dot{U}_{1\_SP} \tag{20}$$

At such frequency, with value depending on the value of mutual inductance (distance between the transmitting and receiving coils), it is possible to achieve a quite high value of the system

efficiency together with peak power transfer. For example, when the system has $M = 5$ μH, which is relevant to 40 cm of distance between coils, then almost 85% of the system efficiency can be achieved at the peak power that is transferred to the load. As it can be further seen in **Figure 7** (right), the value of efficiency naturally depends on the value of the output load. Anyway, it is still possible to achieve an acceptable value of system efficiency even at the sharp change of the output load. Such behavior is mostly welcomed for perspective wireless charging systems, where high transmitting distance, high efficiency, high transferred power, and variable load are required.
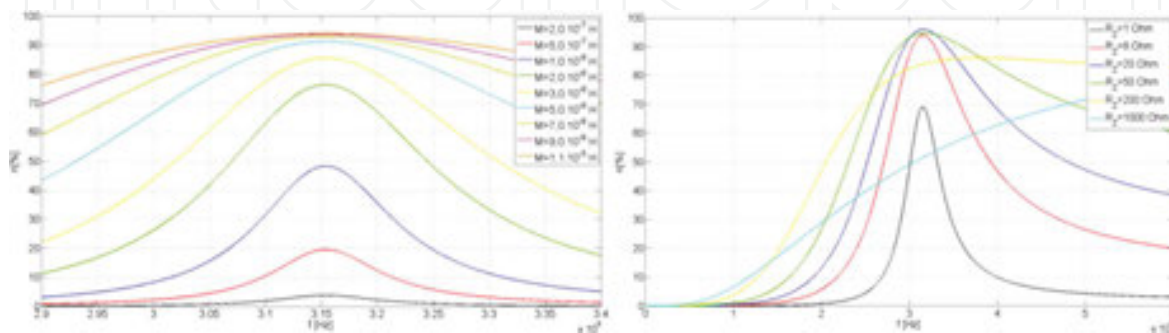

Figure 7. Dependency of efficiency on the series–series coupling (left) and on the output load change at $M = 11$ μH (right).

From the practical point of view, during the design process of the system, it is necessary to know the voltage waveform at compensation capacitors because these components are the most critical. Figures 8 and 9 show voltage dependency for each system component. It can be seen that even for a very low value of the supply voltage (in this case 30 V), the peak voltage at each component multiplies several times. Situation is most critical when the system operates at resonant frequency and also when a low value of mutual inductance is presented. If the input voltage rises, then naturally each particular voltage rises correspondingly too. The selection of the proper capacitor structure and configuration therefore means the most difficult issue. Thus, the previous recommendation for system operation at border resonant frequencies (19) also gives advantages from the system component design point of view. The same is valid
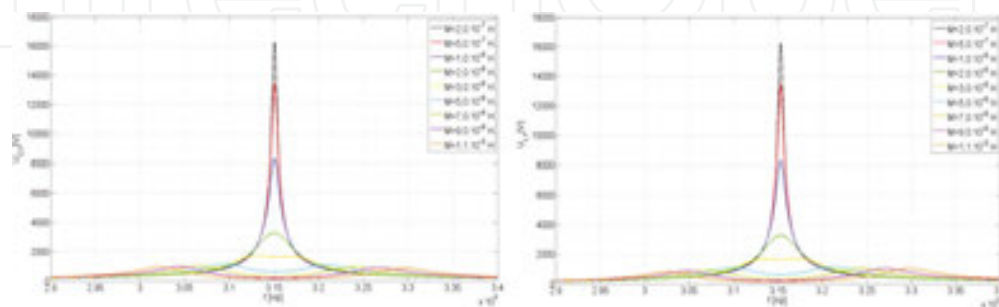

Figure 8. Dependency of voltage on the primary compensation capacitor C_1 (left) and on the primary coil L_1 (right) for series–series coupling.

for the wire selection of the transmitting and receiving coils, when the source and load current show similar dependency, as the previous circuit variables (**Figure 10**).
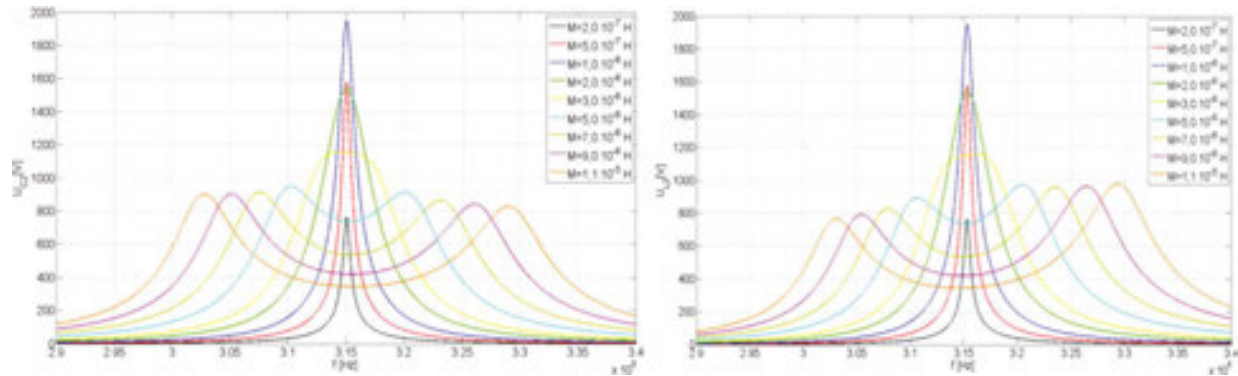

Figure 9. Dependency of voltage on the secondary compensation capacitor C_2 (left) and on the secondary coil L_2 (right) for series–series coupling.
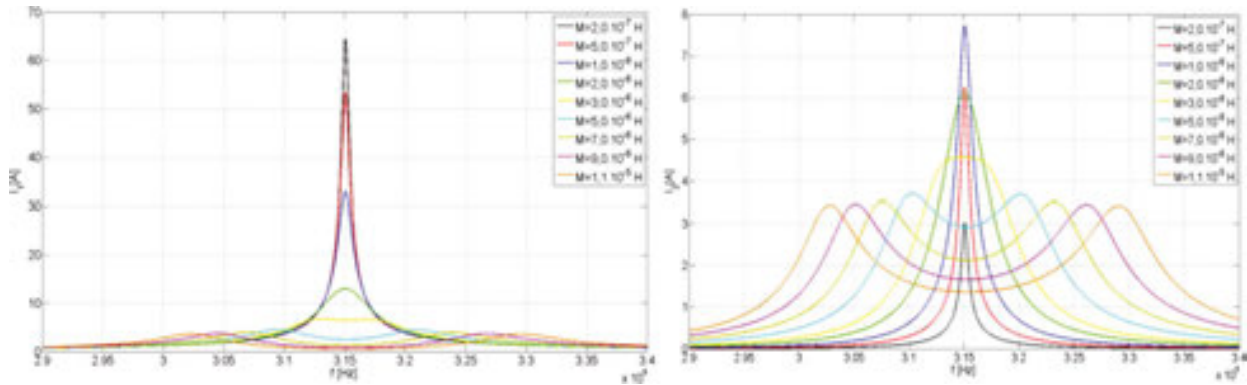

Figure 10. Source current (left) and load current (right) dependency on series–series coupling.

4. Series–parallel resonant coupling of the WET system

Series–parallel compensation means that one capacitor is connected in series to the transmitting coil and the other one is connected in parallel to the receiving coil, see **Figure 11**.

Using the method of loop currents, the impedance matrix of series–parallel compensated circuit can be expressed as follows (24):

$$- j\omega M.\dot{I}_{1\_SP} + \left[R_2 + j\left(\omega L_2 - \frac{1}{\omega C_2} \right) \right].\dot{I}_{2\_SP} + j\frac{1}{\omega C_2}.\dot{I}_{3\_SP} = 0 \tag{21}$$

$$Z_1 = R_1 + j\left(\omega L_1 - \frac{1}{\omega C_1}\right)$$

$$Z_2 = R_2 + j\left(\omega L_2 - \frac{1}{\omega C_2}\right)$$

$$j\frac{1}{\omega C_2}.\dot{I}_{2\_SP} + \left[R_L - j\frac{1}{\omega C_2}\right]\dot{I}_{3\_SP} = 0 \tag{22}$$

$$\begin{bmatrix} \dot{U}_{1\_SP} \\ 0 \\ 0 \end{bmatrix} = \begin{bmatrix} R_1 + j\left(\omega L_1 - \frac{1}{\omega C_1}\right) & -j\omega M & 0 \\ -j\omega M & R_2 + j\left(\omega L_2 - \frac{1}{\omega C_2}\right) & j\frac{1}{\omega C_2} \\ 0 & j\frac{1}{\omega C_2} & R_L - j\frac{1}{\omega C_2} \end{bmatrix} \cdot \begin{bmatrix} \dot{I}_{1\_SP} \\ \dot{I}_{2\_SP} \\ \dot{I}_{3\_SP} \end{bmatrix} \tag{23}$$

$$\begin{bmatrix} \dot{U}_{1\_SP} \\ 0 \\ 0 \end{bmatrix} = \begin{bmatrix} R_1 + j\left(\omega L_1 - \frac{1}{\omega C_1}\right) & -j\omega M & 0 \\ -j\omega M & R_2 + j\left(\omega L_2 - \frac{1}{\omega C_2}\right) & j\frac{1}{\omega C_2} \\ 0 & j\frac{1}{\omega C_2} & R_L - j\frac{1}{\omega C_2} \end{bmatrix} \cdot \begin{bmatrix} \dot{I}_{1\_SP} \\ \dot{I}_{2\_SP} \\ \dot{I}_{3\_SP} \end{bmatrix} \tag{24}$$

If we substitute $Z_1 = R_1 + j\left(\omega L_1 - \frac{1}{\omega C_1}\right)$ and $Z_2 = R_2 + j\left(\omega L_2 - \frac{1}{\omega C_2}\right)$, the circuit currents can be expressed as follows:

$$\dot{I}_1 = \dot{I}_{1\_SP} = \frac{R_2 + j\frac{1}{\omega C_2\left(j\omega C_2 R_L + 1\right)}}{R_1 R_2 + \omega^2 M^2 + j\frac{R_1}{\omega C_2\left(j\omega C_2 R_L + 1\right)}}\dot{U}_{1\_SP} \tag{25}$$

$$\dot{I}_2 = \dot{I}_{2\_SP} = \frac{j\omega M}{R_1 R_2 + \omega^2 M^2 + j\frac{R_1}{\omega C_2\left(j\omega C_2 R_L + 1\right)}}\dot{U}_{1\_SP} \tag{26}$$

$$\dot{I}_3 = \dot{I}_{2\_SP} - \dot{I}_{3\_SP} = \frac{-\omega^2 C_2 R_L M}{\left(R_1 R_2 + \omega^2 M^2\right)\left(j\omega C_2 R_L + 1\right) + j\frac{R_1}{\omega C_2}}\dot{U}_{1\_SP} \tag{27}$$

$$\dot{I}_4 = \dot{I}_{3\_SP} = \frac{j\omega M}{\left(R_1 R_2 + \omega^2 M^2\right)\left(j\omega C_2 R_L + 1\right) + j\dfrac{R_1}{\omega C_2}}\dot{U}_{1\_SP} \tag{28}$$
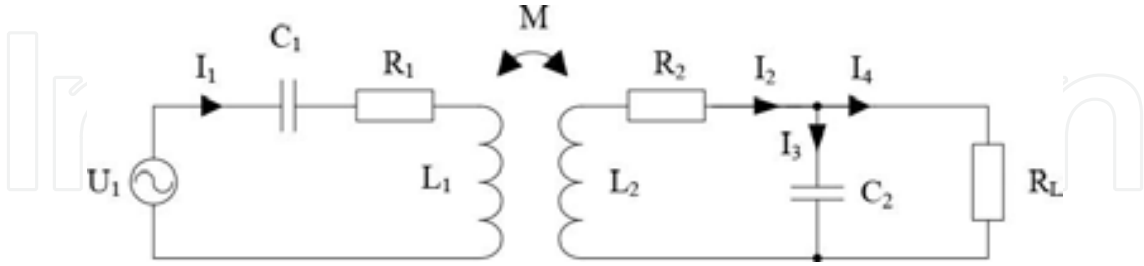

Figure 11. Equivalent circuit of the series–parallel compensated WET system.

Compared with the series–series compensation, in this case the reactance of capacitor C_2 influences circuit variables when circuit is powered by the resonant frequency because C_2 is in parallel to the load resistance R_L. In this case, the power consumption, output power, and efficiency can be calculated in the same way as in the case of series–series compensation (Eqs. (28)–(31)).

$$\dot{S}_{IN\_SP} = \dot{I}_1 \dot{U}_{1\_SP} = \frac{Z_2 + j\dfrac{1}{\omega C_2\left(j\omega C_2 R_L + 1\right)}}{Z_1 Z_2 + \omega^2 M^2 + j\dfrac{Z_1}{\omega C_2\left(j\omega C_2 R_L + 1\right)}}\dot{U}_{1\_SP}^2 \tag{29}$$

$$P_{OUT\_SP} = R_L \cdot \left|\dot{I}_4\right|^2 = \left|\frac{-\omega^2 M^2 R_L}{\left[\left(Z_1 Z_2 + \omega^2 M^2\right)\left(j\omega C_2 R_L + 1\right) + j\dfrac{Z_1}{\omega C_2}\right]^2}\dot{U}_{1\_SP}^2\right| \tag{30}$$

$$\eta = \left|\frac{P_{OUT\_SP}}{\dot{S}_{IN\_SP} \cdot \cos(\varphi)}\right|$$

$$= \left|\frac{-\omega^2 M^2 R_L}{\left[Z_2\left(j\omega C_2 R_L + 1\right) + j\dfrac{1}{\omega C_2}\right]\left[\left(Z_1 Z_2 + \omega^2 M^2\right)\left(j\omega C_2 R_L + 1\right) + j\dfrac{Z_1}{\omega C_2}\right] \cdot \cos(\varphi)}\right| \tag{31}$$

$$\cos(\varphi) = \frac{\Re\left(\dot{S}_{IN}\right)}{\left|\dot{S}_{IN}\right|} = \frac{\Re\left(\dfrac{Z_2 + j\dfrac{1}{\omega C_2\left(j\omega C_2 R_L + 1\right)}}{Z_1 Z_2 + \omega^2 M^2 + j\dfrac{Z_1}{\omega C_2\left(j\omega C_2 R_L + 1\right)}}\dot{U}_{1\_SP}^2\right)}{\left|\dfrac{Z_2 + j\dfrac{1}{\omega C_2\left(j\omega C_2 R_L + 1\right)}}{Z_1 Z_2 + \omega^2 M^2 + j\dfrac{Z_1}{\omega C_2\left(j\omega C_2 R_L + 1\right)}}\dot{U}_{1\_SP}^2\right|} \tag{32}$$

The graphical interpretations of the mentioned variables are introduced depending on frequency as well as M (Figures 12–14). Small change of frequency from resonant frequency causes that power consumption and power delivered to the load are significantly reduced (**Figure 12**). Considering similar dependency for efficiency, it shows no change when frequency is being changed (**Figure 13**, left). This is advantageous when power delivery at constant efficiency needs to be managed.
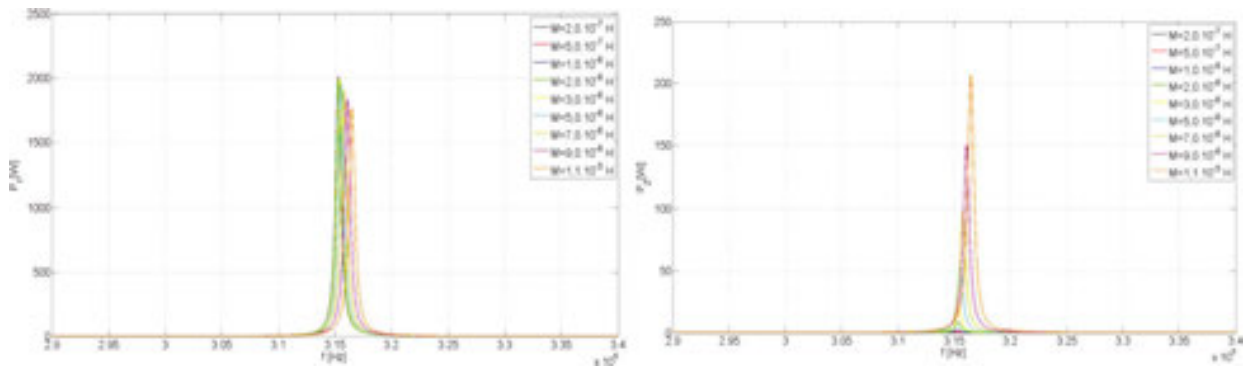

Figure 12. Input power (left) and output power (right) dependency on series–parallel coupling.

On the other hand, the poor efficiency is the highest disadvantage. Let now consider a different situation, when M reaches higher values (reduction of distance between coils). **Figure 13** (right) shows that the efficiency is significantly increased. This means that the best efficiency can be achieved for a short distance, while power transfer to the load is comparable with power transfer for series–series compensation, see **Figure 14** (left).

Efficiency also depends on the change of the load value. For series–parallel compensation, the higher efficiency can be achieved at higher values of load resistance (reduction of delivered power). **Figure 14** (right) shows dependency of system efficiency on series–parallel compensation at constant $M = 11\ \mu H$ during load change. It can be seen that for lower transfer distances ($M = 11\ \mu H$ is relevant to 20 cm of mutual distance), the efficiency can be kept at high values even for a wide range of load (**Figure 14**).
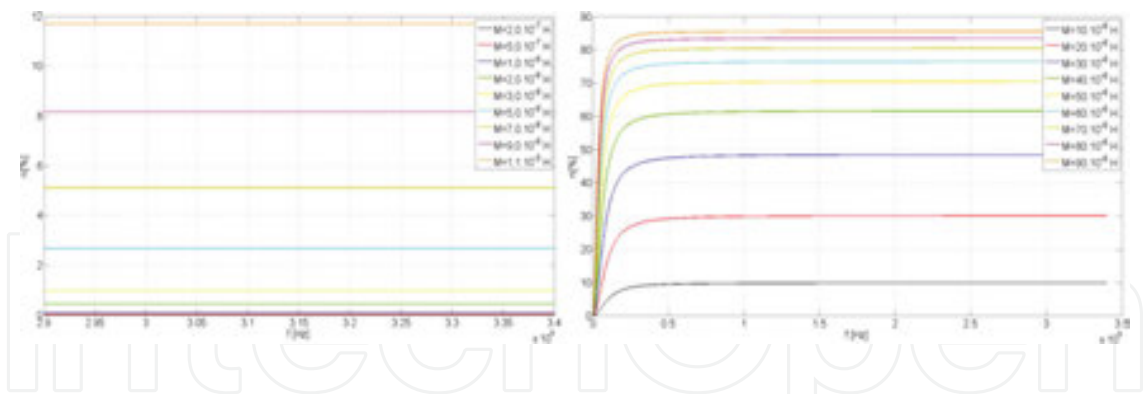
Figure 13. Dependency of efficiency on series–parallel coupling (left) and on higher values of mutual inductance (right).
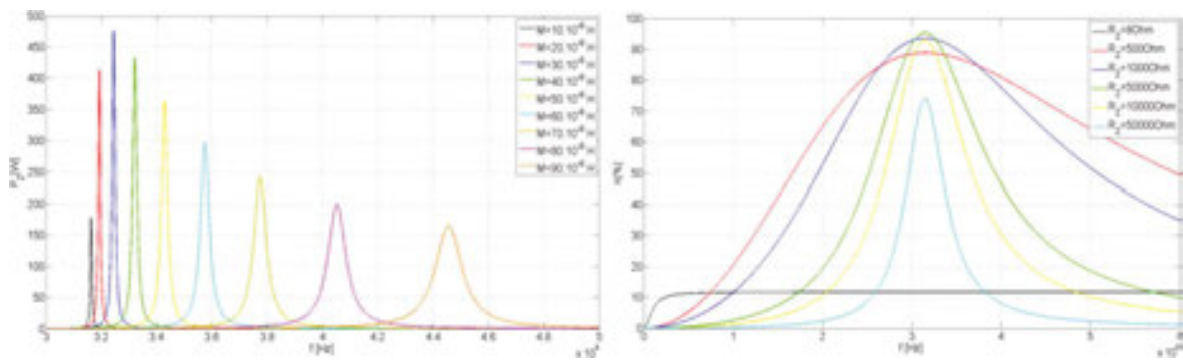

Figure 14. Dependency of the output power on higher values of mutual inductance (left) and dependency of efficiency (right) on variable load at constant $M = 11 \, \mu H$.

Voltage on capacitor C_1 (**Figure 15**) in the series–parallel compensated system also achieves high levels. A decrease or increase in the switching frequency not only reduces the voltage stresses on the capacitor, but also significantly reduces the transmitted power. The same situation is valid for the voltage on coil L_1.
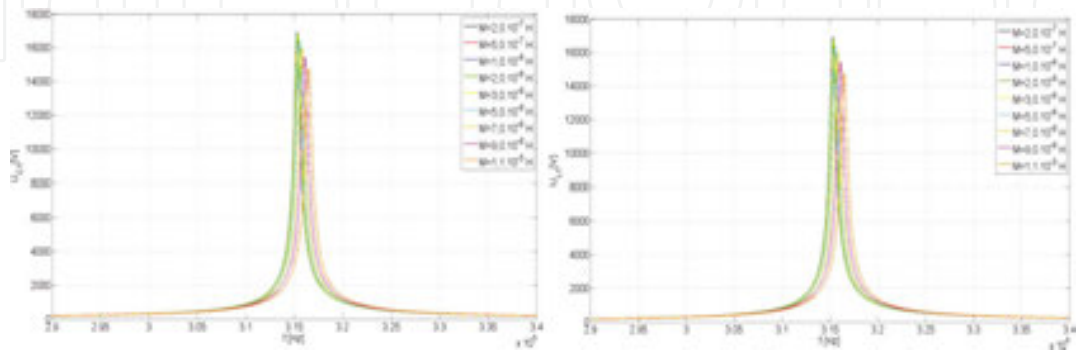

Figure 15. Dependency of voltage on the primary compensation capacitor C_1 (left) and on the primary coil L_1 (right) for series–parallel coupling.

Voltage on capacitor C_2 (**Figure 16**, left) is the voltage on the resistive load and the receiver coil L_2 too because they are connected in parallel. In contrast to the voltage on capacitor C_1, the voltage on capacitor $C2$ is smaller. This voltage is increased when value of M is increased too, but only up to a certain value of the mutual inductance, in our case it is 30 µH. The voltage on capacitor C_2 falls above this value. Capacitor C_2 does not have to be necessary designed for high voltage stresses, which reduces the overall costs of the system.
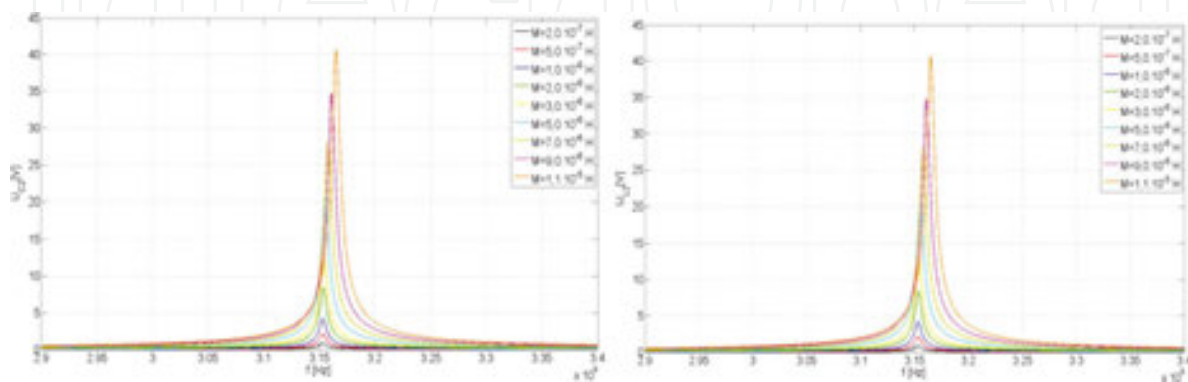

Figure 16. Dependency of voltage on the secondary compensation capacitor C_2 (left) and on the secondary coil L_2 (right) for series–parallel coupling.

Frequency dependencies of circuit currents are shown in Figures 17 and 18. It can be seen (**Figure 17**, left) that I_1 decreases with the increase in the mutual inductance and its peak point is shifted to higher frequencies contrary to resonant frequency.

Figures 17 (right) and 18 show the current of the receiving coil I_2, divided into current of capacitor C_2 and a load resistance R_L. Because the value of load resistor is realativelly small, $R_L = 8\ \Omega$, the majority of coil current flows just through load resistance, I_4. Current I_3 of the secondary capacitor C_2 has smaller magnitude. With the increase in the mutual inductance, the maximum of all currents rises.
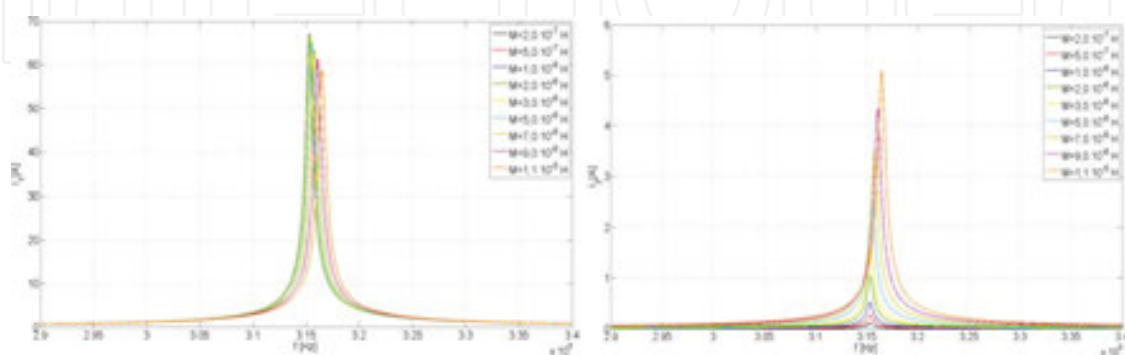

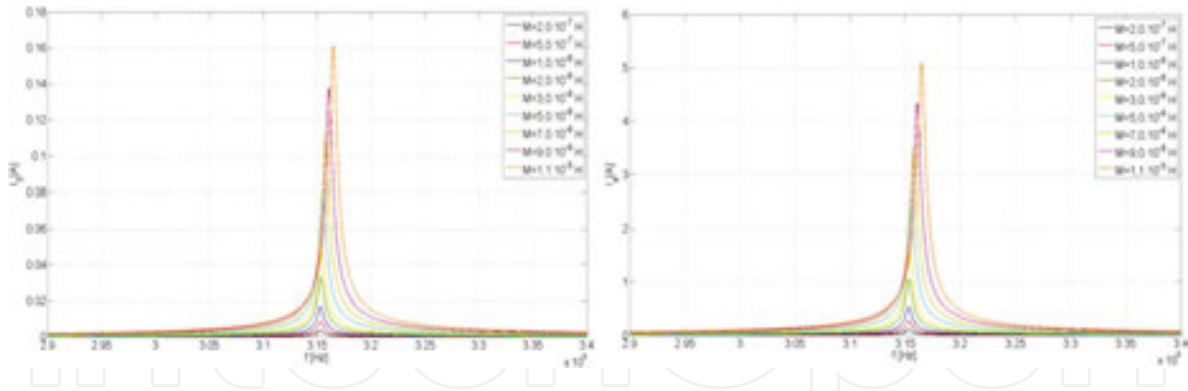**Figure 17.** Dependency of current I_1 (left) and I_2 (right) on series–parallel coupling.

Figure 18. Dependency of current I_3 (left) and I_4 (right) on series–parallel coupling.

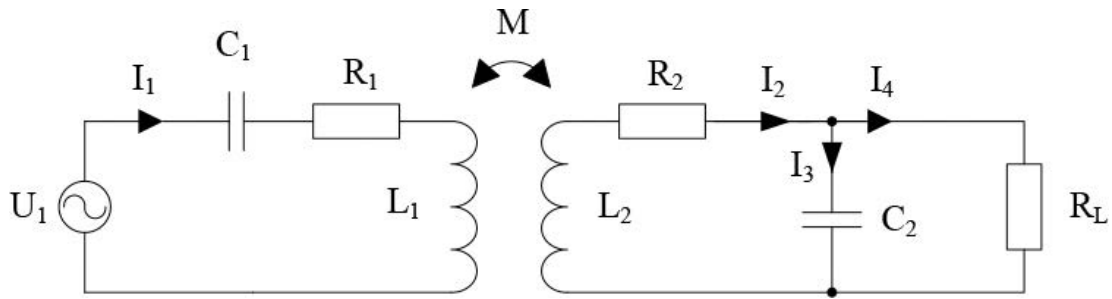## 5. Parallel–series resonant coupling of the WET system

Figure 19. Equivalent circuit of the parallel–series compensated WET system.

Equivalent circuit for parallel–series compensation is shown in **Figure 19**. Capacitor C_1 is connected in parallel to the power supply and transmitting coil. The secondary consists of series connection of L_2–C_2–R_L.

With consideration of equivalent circuit shown in **Figure 9**, it is possible to express a system of three linear equations with three unknown parameters (14).

$$
\begin{bmatrix} \dot{U}_{1\_PS} \\ 0 \\ 0 \end{bmatrix} = \begin{bmatrix} -j\dfrac{1}{\omega C_1} & j\dfrac{1}{\omega C_1} & 0 \\ j\dfrac{1}{\omega C_1} & R_1 + j\omega L_1 - j\dfrac{1}{\omega C_1} & -j\omega M \\ 0 & -j\omega M & R_2 + R_L + j\left(\omega L_2 - \dfrac{1}{\omega C_2}\right) \end{bmatrix} \cdot \begin{bmatrix} \dot{I}_{1\_PS} \\ \dot{I}_{2\_PS} \\ \dot{I}_{3\_PS} \end{bmatrix}
\tag{33}
$$

Equation (32) gives relatively complicated results and therefore some simplifying substitution should be applied: $Z_1 = R_1 + j\left(\omega L_1 - \frac{1}{\omega C_1}\right)$ and $Z_2 = R_2 + R_L + j\left(\omega L_2 - \frac{1}{\omega C_2}\right)$. The aimed winding and load currents are determined by Eqs. (33)–(35):

$$\dot{I}_1 = \dot{I}_{1\_PS} = \frac{j\omega C_1 (Z_1 Z_2 + \omega^2 M^2)}{Z_1.Z_2 + (\omega M)^2 + j\dfrac{Z_2}{\omega C_1}} \dot{U}_{1\_PS} \tag{34}$$

$$\dot{I}_2 = \dot{I}_{1\_PS} - \dot{I}_{2\_PS} = \frac{j\omega C_1 (Z_1 Z_2 + \omega^2 M^2) - Z_2}{Z_1.Z_2 + (\omega M)^2 + j\dfrac{Z_2}{\omega C_1}} \dot{U}_{1\_PS} \tag{35}$$

$$\dot{I}_4 = \dot{I}_{3\_PS} = \frac{j\omega M}{Z_1 Z_2 + (\omega M)^2 + j\dfrac{Z_2}{\omega C_1}} \dot{U}_{1\_PS} \tag{36}$$
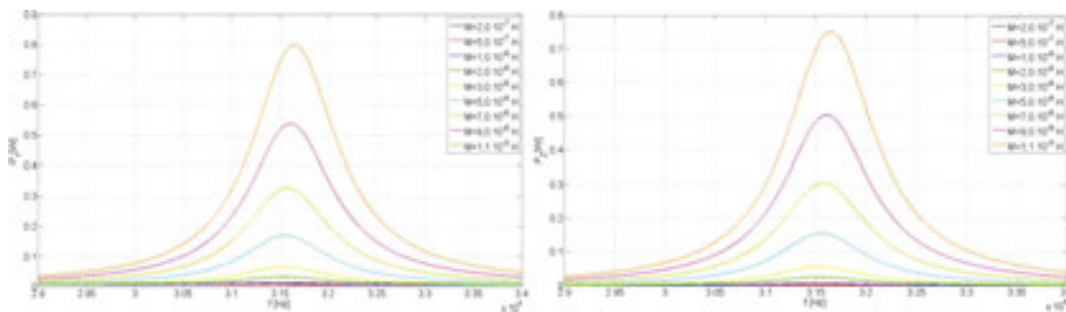

Figure 20. Input power (left) and output power (right) dependency on series–parallel coupling.

The input and output powers are then found in the same way as from previous analyses (36)–(37).

$$\dot{S}_{IN\_PS} = \dot{I}_1 \dot{U}_{1\_PS} = \frac{j\omega C_1 (Z_1 Z_2 + \omega^2 M^2)}{Z_1.Z_2 + (\omega M)^2 + j\dfrac{Z_2}{\omega C_1}} \dot{U}_{1\_PS}^2 \tag{37}$$

$$P_{OUT\_SP} = R_L.\left|\dot{I}_4\right|^2 = \left|\frac{-\omega^2 M^2 R_L}{\left[Z_1 Z_2 + (\omega M)^2 + j\dfrac{Z_2}{\omega C_1}\right]^2} \dot{U}_{1\_SP}^2\right| \tag{38}$$

where

$$\cos(\varphi) = \frac{\Re\left(\dot{S}_{IN}\right)}{\left|\dot{S}_{IN}\right|} = \frac{\Re\left(\dfrac{j\omega C_1(Z_1 Z_2 + \omega^2 M^2)}{Z_1.Z_2 + (\omega M)^2 + j\dfrac{Z_2}{\omega C_1}}\dot{U}_{1\_PS}^2\right)}{\left|\dfrac{j\omega C_1(Z_1 Z_2 + \omega^2 M^2)}{Z_1.Z_2 + (\omega M)^2 + j\dfrac{Z_2}{\omega C_1}}\dot{U}_{1\_PS}^2\right|} \tag{39}$$

The graphical interpretation of Eq. (37) is shown in **Figure 20**. It shows that any frequency deviation from the resonant state reduces the power delivered to the load. However, in this case the system is less sensitive to frequency change as compared to the series–parallel compensation.

The power delivery to the load for this type of compensation and for the selected operational variables (load, mutual inductance, etc.) is, when compared to the previous types, very poor. Efficiency dependency (**Figure 21**) is comparable to series–parallel compensation, whereby the higher the value of the mutual inductance is, the higher efficiency can be achieved. Similarly, as for series–parallel compensation it is expected that the parallel–series compensation type is more valuable for higher values of mutual inductances, and thus for applications, where distance is not the primary attribution of the WET system.

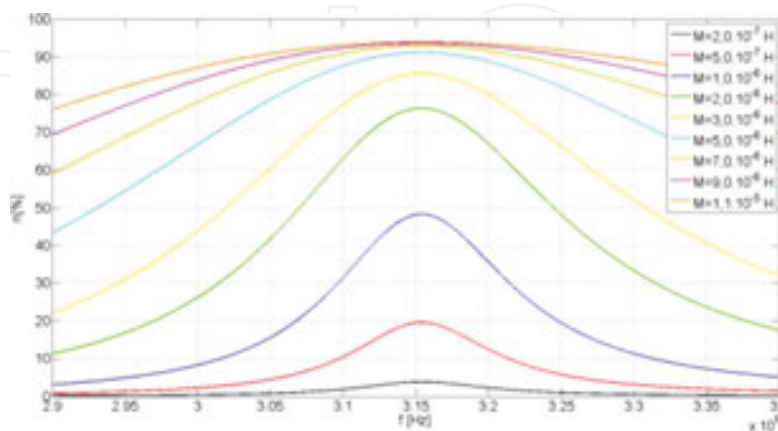The advantage of this configuration is the low electrical stress of individual components (Figures 22 and 23).

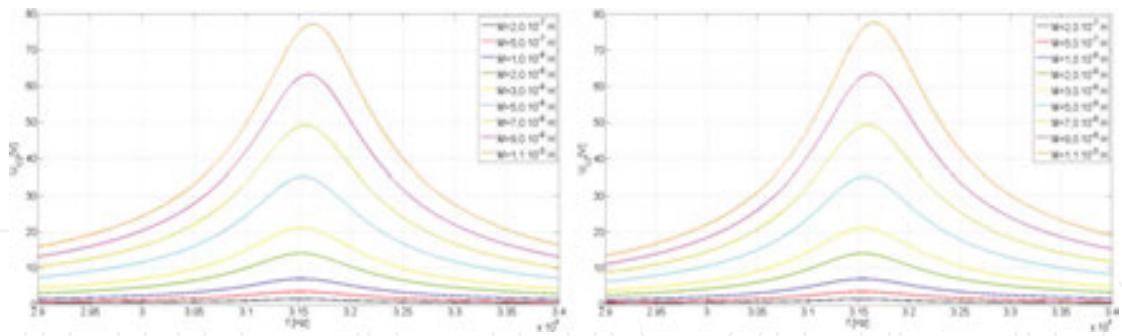**Figure 21.** Dependency of efficiency on parallel–series coupling.

Figure 22. Dependency of voltage on the secondary compensation capacitor C_2 (left) and on the secondary coil L_2 (right) for parallel–series coupling.

6. Parallel–parallel resonant coupling of the WET system

Equivalent circuit of the system is shown in **Figure 23**. Both compensation capacitors are connected in parallel to the transmitting and receiving coils. Unlike the previous topologies, this model forms the system of four linear equations with four unknown parameters (26):
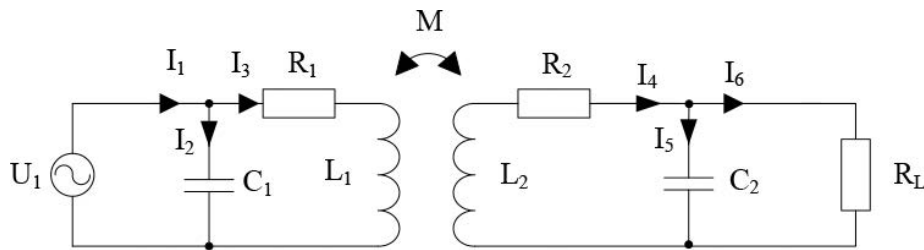

Figure 23. Equivalent circuit of the parallel–parallel compensated WET system.

$$\begin{bmatrix} \dot{U}_{1\_PS} \\ 0 \\ 0 \\ 0 \end{bmatrix} = \begin{bmatrix} -j\dfrac{1}{\omega C_1} & j\dfrac{1}{\omega C_1} & 0 & 0 \\ j\dfrac{1}{\omega C_1} & R_1 + j\omega L_1 - j\dfrac{1}{\omega C_1} & -j\omega M & 0 \\ 0 & -j\omega M & R_2 + j\omega L_2 - j\dfrac{1}{\omega C_2} & j\dfrac{1}{\omega C_2} \\ 0 & 0 & j\dfrac{1}{\omega C_2} & R_L - j\dfrac{1}{\omega C_2} \end{bmatrix} \cdot \begin{bmatrix} \dot{I}_{1\_PP} \\ \dot{I}_{2\_PP} \\ \dot{I}_{3\_PP} \\ \dot{I}_{4\_PP} \end{bmatrix} \qquad (40)$$

After substitution $Z_1 = R_1 + j\left(\omega L_1 - \frac{1}{\omega C_1}\right)$, $Z_2 = R_2 + j\left(\omega L_2 - \frac{1}{\omega C_2}\right)$, and $Z_3 = R_L - j\left(\frac{1}{\omega C_2}\right)$, the most important circuit variables can be obtained as follows:

$$\dot{I}_1 = \dot{I}_{1\_PP} = \left[j\omega C_1 + \cfrac{1}{\left(Z_1 + j\cfrac{1}{\omega C_1} \right) + \cfrac{\omega^4 C_2^{\ 2} Z_3 M^2}{\omega^2 C_2^{\ 2} Z_2 Z_3 + 1}} \right] \dot{U}_{1\_PP} \tag{41}$$

$$\dot{I}_6 = \dot{I}_{4\_PP} = \cfrac{-\cfrac{M}{Z_3 C_2}}{\left(Z_1 + j\cfrac{1}{\omega C_1} \right)\left(\cfrac{1}{\omega^2 C_2^{\ 2} Z_3} + Z_2 \right) + (\omega M)^2} \dot{U}_{1\_PP} \tag{42}$$

$$P_{OUT\_PP} = R_L \cdot \left| \dot{I}_6 \right|^2 = \left| \cfrac{R_L \left(-\cfrac{M}{Z_3 C_2} \right)^2}{\left[\left(Z_1 + j\cfrac{1}{\omega C_1} \right)\left(\cfrac{1}{\omega^2 C_2^{\ 2} Z_3} + Z_2 \right) + (\omega M)^2 \right]^2} \right| \dot{U}_{1\_PP}^2 \tag{43}$$

$$\eta = \left| \cfrac{P_{OUT\_SP}}{\dot{S}_{IN\_SP} \cdot \cos(\varphi)} \right|$$

$$= \left| \cfrac{R_L M^2}{Z_3^2 C_2^2 \left[j\omega C_1 \left[\left(Z_1 + j\cfrac{1}{\omega C_1} \right) + \cfrac{\omega^4 C_2^{\ 2} Z_3 M^2}{\omega^2 C_2^{\ 2} Z_2 Z_3 + 1} \right]^2 + \left(Z_1 + j\cfrac{1}{\omega C_1} \right) + \cfrac{\omega^4 C_2^{\ 2} Z_3 M^2}{\omega^2 C_2^{\ 2} Z_2 Z_3 + 1} \right] \cos(\varphi)} \right| \tag{44}$$

Regarding of the system performance, it is similar to characteristics found for nonresonant magnetic coupling. Thus, this type of compensation is not suitable for applications where simultaneously high power with high efficiency is required to transmit power on large distances.

7. Conclusion

Based on the study, a table (**Table 1**) of key operating features for the discussed compensation topologies is composed. **Table 1** only covers the system behavior at chosen frequency and distance range while considering constant supply voltage and low value of loading resistance.

In **Table 1**, attribute "**A**" marks the ability to transfer high power to the load, attribute "**B**" means that the system operates with maximal efficiency at the same time when it transmits

the maximal power. Attribute "**C**" distinguishes the compensation topology with higher frequency sensitivity and finally attribute "**D**" indicates the ability to reach theoretical transmitting efficiency, possibly higher than 90%.

Compensation	Evaluated categories			
	A	B	C	D
None		×		
Series–series	×		×	×
Series–paralel	×		×	
Parallel–series		×	×	×
Parallel–parallel		×		

Table 1. Overview of key performance features.

According to **Table 1**, the noncompensated system and the system with parallel–parallel compensation are both inappropriate for any type of wireless charger working at large distance and higher level of transmitting energy. On the other hand, they achieve maximum efficiency precisely at the moment they deliver maximum power. Hence, they should be used for low-cost micropower battery chargers which moreover require no frequency tuning.

In contrast to other topologies, the series–series compensation provides relatively high power even through a very large working air gap, but the efficiency reaches its peak only at off-resonant frequencies. The system should be therefore operated at compromise between useable energy and the transmitting efficiency. Despite this fact, the system is suitable for high-power chargers for electric vehicles.

The series–parallel compensation forms more disadvantages than advantages and therefore cannot be recommended for any battery charger. With respect to all evaluated categories, the parallel–series compensation provides the best performance, but from power delivering point of view, this solution is much worse. However, it could be recommended for high-end frequency tuned micropower battery chargers.

Acknowledgements

Author details

Michal Frivaldsky[*], Pavol Spanik, Peter Drgona, Viliam Jaros and Marek Piri

*Address all correspondence to: michal.frivaldsky@fel.uniza.sk

Department of Mechatronics and Electronics, Faculty of Electrical Engineering, University of Zilina, Slovakia

References

[1] Wang, C.-S.; Stielau, O.H.; Covic, G.A. Design Considerations for a Contactless Electric Vehicle Battery Charger. IEEE Transactions on Industrial Electronics. 2005;52(5):1308–1314.

[2] Hui, S.Y.R.; Zhong, W.; Lee, C.K. A Critical Review of Recent Progress in Mid-Range Wireless Power Transfer. IEEE Transactions on Power Electronics. 2014;29:4500–4511.

[3] Covic, G.A.; Boys, J.T. Modern Trends in Inductive Power Transfer for Transportation Applications. IEEE Journal of Emerging and Selected Topics in Power Electronics. 2013;1:28–41.

[4] Zhai, H.; Pan, H.K.; Lu, M. A practical wireless charging system based on ultra-wideband retro-reflective beam forming. Antennas and Propagation Society International Symposium. 2010:1–4.

[5] Kim, S.; Jung, D.H.; Kim, J.J.; Bae, B.; Kong, S.; Ahn, S.; Kim, J.; Kim, J. High-Efficiency PCB- and Package-Level Wireless Power Transfer Interconnection Scheme Using Magnetic Field Resonance Coupling. IEEE Transactions on Components Packaging and Manufacturing Technology. 2015;5(7):863–878.

[6] Covic, G.A.; Boys, J.T. Inductive Power Transfer. Proceedings of the IEEE. 2013;101(6): 1–14.

[7] Kurs, A.; Karalis, A.; Moffatt, R.; Joannopoulos, J.D.; Fisher, P.; Soljacic, M. Wireless Power Transfer via Strongly Coupled Magnetic Resonances. Science. 2007;317(5834): 83–86.

[8] Peschiera, B.; Williamson, S.S. Review of inductive power transfer technology for electric and plug-in hybrid electric vehicles, in Industrial Electronics Society. IECON 2013—39th Annual Conference of the IEEE. 2013:4672–4677.

[9] Dai, J.; Ludois, D.C. A Survey of Wireless Power Transfer and a Critical Comparison of Inductive and Capacitive Coupling for Small Gap Applications. IEEE Transactions on Power Electronics. 2015;30(11):6017–6029.